# Large-scale flood detection in the Pearl River basin based on GEE and time-series Sentinel-1 SAR images

Bofei Zhao[1], Haigang Sui[1]

[1] State Key Laboratory of Information Engineering in Surveying, Mapping and Remote Sensing, Wuhan University, China - bowie.zhao@whu.edu.cn

**Commission III**

**KEY WORDS:** SAR, GEE, Flood Detection, Sentinel-1, Large-scale.

**ABSTRACT:**

Due to its wide scope, rapid development and high hazard, remote sensing images with a single time phase and local area coverage cannot meet the needs of large-scale flood detection. The problem of large-scale flooding emergency detection can be well solved by using Google Earth Engine (GEE) platform, which has the characteristics of fast data computing speed, easy image retrieval and rich remote sensing data. In this paper, we propose a method for flood detection using Sentienl-1 imagery based on the GEE platform, which can quickly accomplish a large scale flood detection. The method was validated in a flooding event that occurred around the Pearl River basin, China in June 2022. It shown that using the proposed method can not only meet the needs of basin-wide flood detection, but also extract information on the temporal dimension of the flood development status.

## 1. INTRODUCTION

Every year, a large number of flooding events occur around the world, and it is very important to obtain accurate and fast flooding information to reduce the damage. Remote sensing technology is an important tool for more thorough perception and understanding of natural disasters, because combining multi-source remote sensing images enables accurately extract flood disaster information. Mirela et al. [25] provides new ideas for the extraction of floods of short duration, which used a combined multi-satellite approach to rapidly detect occurring floods. Chohan et al. [7] combined remote sensing (RS) and Geographic Information System (GIS) technology to analyse the sinuosity index of the river channel, providing auxiliary information on the river morphology for the flood disaster management. In addition, flood disaster research based on geospatial information, such as identification of homogeneous areas of flash floods[33] and assessment of susceptibility to mountain torrents[32], is helpful for flood disaster management. At present, remote sensing satellite resources are becoming more and more abundant. Higher resolution of remote sensing images and more adequate time series images are beneficial for more comprehensive and finer monitoring and assessment of flooding hazards. How to use long-time series and large-scale remote sensing images to realize flood disaster monitoring at the basin level is an important research topic.

Due to the strong computing power, fast data processing, and comprehensive database, more and more scholars conduct remote sensing image processing research based on Google Earth Engine (GEE). Gong et al. [19] developed the global land cover data product (GLASS-GLC) with 5 km spatial resolution and 34 years by using the Global Land Surface Characteristic Reference Dataset (GLASS CDR) from 1982 to 2015 with the GEE. Canty et al. [3] analysed long time series of dual-polarized SAR images in the GEE platform to implement applications for monitoring changes in various human activities and natural disasters. Ben et al. [9] innovatively used the GEE platform for rapid detection of flooding events on Sentinel-1 SAR images and Landsat images. Guo et al. [2] analysed the changes of water bodies within one year using Sentinel 1 and Sentinel 2 remote sensing images based on GEE, which effectively detected different types of flood information.

Yan et al. [31] analysed the dynamic change information of water bodies in the Yangtze River basin between 2016 and 2020 based on the results of multi-temporal water body extraction from SAR images of long time series. Peter et al. [23] proposed a flood depth estimation tool (FwDET) that can provide flood depth calculations for flood hazards in a very short period of time. Therefore, it is feasible to monitor flood with large scale SAR images in GEE platform.

The core of flood monitoring is to detect the changing state of water bodies in the same location. By studying the change detection algorithm of SAR images, many scholars have realized the direct detection of the change state of water bodies in remote sensing. SAR change detection includes methods that implement change detection based on difference images (DI), and methods that use deep convolutional networks to extract diachronic features and predict change information. DI-based change detection methods, such as PCA-Kmeans [4], GaborTLC [15], NRELM [11], relies on the differentiation of DI features and does not work well in regions with complex backgrounds. The change detection (CD) method based on deep convolutional network can meet the tasks of heterogeneous image change detection [30] and building change detection [20], but it is generally limited by the difficulty of sample acquisition. The test data of these methods are generally remote sensing images with a single background, which do not match with the actual application scenarios [12].

At present, the most dominant flood detection method is to extract the multi-temporal water body and then compare the water body change state. The methods of water body extraction using remote sensing images are mainly divided into two categories, threshold segmentation method and deep learning method. By testing the water extraction accuracy of SAR images with HRNet [27], DenseNet [14], SegNet [1], Resnet [13], DeepLab V3+ [5], bimodal threshold segmentation, and the Otsu algorithms [22], Dong et al. [10] chose HRNet as the optimal water extraction method to made a detailed analysis of the summer flood of Poyang Lake in China in 2020. Wang et al. [28] proposed a deep convolutional network for water extraction from SAR images (FWENet), and the experimental

results showed that the accuracy of FWENet water extraction was better than the classical deep learning networks UNet, UNet++ and DeepLab v3 algorithms, and the method was used to successfully analyze the development of flooding in Poyang Lake in 2022. The deep learning algorithm for water extraction also achieves good accuracy in optical remote sensing images [8, 16, 17, 29]. But they all require a large number of labelled samples and the network model is computationally intensive.

Compared to advanced deep learning algorithms, the improved threshold segmentation method has the advantages of simplicity and speed. Chini et al. [6] proposed a hierarchical split-based approach to achieve a parametric fit of two types of distribution functions for background and target. Due to the difference of backscattering between water bodies and other classes in SAR images, the threshold method to extract water bodies in SAR images has the advantage of simplicity and speed. Nagai et al. [21] created a new water body index (NoBADI) that removes seasonally fluctuating uncertain water bodies in flooded water bodies. Liang and Liu [18] proposed a new local threshold method to extract water body boundaries by finely dividing according to the GAMMA distribution of each feature and water, and achieved high accuracy water body boundary extraction by hydrological constraint post-processing. Vanama et al. [26] proposed a Normalized Change Index (NCI) to extract the flood extent by calculating the difference in backscatter coefficients between the before and after flood in combination with the Otsu threshold method.

However, the large-scale flood detection using remote sensing imagery is subject to the complex pre-processing process and large amount of computation. In addition, the threshold method of water body extraction faces the problem of difficulty in distinguishing mountain shadows from water bodies. The above problems can be solved using the GEE platform as the GEE platform has other geospatial data and long-time series of remote sensing images. Flood detection based on the GEE platform not only avoids the pre-processing of the dataset, but also enables fast processing of multiple images. Meanwhile, the shadow area of the mountain can be effectively removed from the water body extraction results with the terrain data.

The article proposes a large scale remote sensing flood detection method, which is based on the long time series SAR images of GEE platform to achieve the identification and distinction between flooded water bodies and permanent water body areas. The example of the study is the flooding that occurred in the Pearl River Basin of Guangdong Province in July 2022. Through the experimental results, it is found that the method in this paper can achieve the extraction and type identification of flooded water bodies in large areas.

## 2. DATA AND METHODS

The Pearl River is the largest river system in southern China, with the geographical range of 22°8'N~25°39'N and 103°57'E~113°27'E. It is composed of four separate river systems: the Xi River (originating from the Yunnan-Guizhou Plateau), the Liuxi River (originating from Conghua City in Guangdong Province), the Beijiang River, and the Dongjiang River (both originating from Jiangxi Province). These four rivers join up in Guangzhou, flow for about 70 kilometres (43.5 miles), and then pour into the South Sea.

Due to continuous heavy rainfall, Yingde City in the Pearl River Basin experienced a major flood around June 20, 2022. Other cities in the Pearl River Basin, such as Shaoguan City, and Qingyuan City, also suffered severe floods. Secondary disasters such as mountain floods, road damage, flooding of farmland, and urban waterlogging occurred in many places.

It is of great significance to use the advantages of remote sensing for large-scale observation to monitor flood disasters in the basin. Therefore, this paper takes this flood disaster as the study area, as shown in Figure 1. In order to verify the effectiveness of the method, two severely affected areas (Yingde City and Qingyuan City, Guangdong) were selected for more detailed analysis, as shown in the two red rectangles in Figure 1.

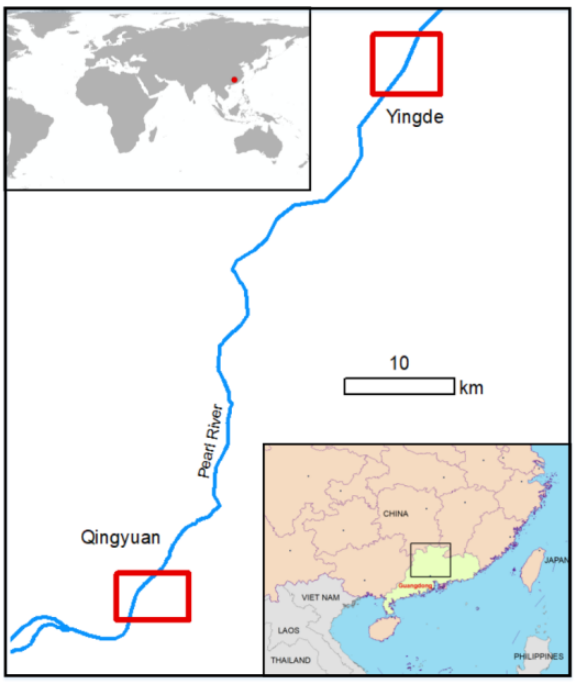


**Figure 1 The location of Pearl River in China.**

The experimental data are ESA Sentinel-1 C-band dual-polarization (VV and VH) SAR data. This collection provided by the GEE is the corrected and ortho-corrected Ground Range Detected (GRD) product generated by the Sentinel-1 Toolbox. The time-series information of SAR images is an important factor in determining the type of water bodies. The GEE platform has powerful computing performance and fast data retrieval capability. In order to calculate the frequency of water bodies, the experimental data includes 70 Sentinel-1 data covering the study area from January 4, 2022 to June 26, 2022. Based on the GEE pre-processing, the data were terrain corrected and Refine Lee filtered. The details of the data are shown in Table 1

| Sentinel-1 | |
|---|---|
| Acquisition mode | IW |
| Polarization | VV & VH |
| Swath | GRD |
| Pixel spacing (m) | 10 |
| Spatial resolution(m) | 20×22 |
| Date of Acquisition | |
| 20220104(Pre-flood) | 20220109(Pre-flood) |
| 20220116(Pre-flood) | 20220121(Pre-flood) |
| 20220128(Pre-flood) | 20220202(Pre-flood) |
| 20220209(Pre-flood) | 20220214(Pre-flood) |
| 20220221(Pre-flood) | 20220226(Pre-flood) |
| 20220305(Pre-flood) | 20220310(Pre-flood) |
| 20220310(Pre-flood) | 20220317(Pre-flood) |

| | |
|---|---|
| 20220322(Pre-flood) | 20220329(Pre-flood) |
| 20220403(Pre-flood) | 20220410(Pre-flood) |
| 20220415(Pre-flood) | 20220422(Pre-flood) |
| 20220427(Pre-flood) | 20220504(Pre-flood) |
| 20220509(Pre-flood) | 20220516(Pre-flood) |
| 20220521(Pre-flood) | 20220528(Pre-flood) |
| 20220602(Pre-flood) | 20220609(Pre-flood) |
| 20220614(During-flood) | 20220621(During-flood) |
| 20220626(During-flood) | 20220703(Post-flood) |
| 20220708(Post-flood) | 20220715(Post-flood) |
| 20220720(Post-flood) | 20220727(Post-flood) |

**Table 1.Sentinel-1 data used for 2022 Pearl River basin flood mapping**

The flow chart of the proposed method is shown in Figure 2. After data selection and pre-processing, all time-series SAR images covering the study area from January-July 2022 were obtained. In order to better utilize the dual polarization information of the sentinel images, the Sentinel-1 Dual-Polarized Water Index (SDWI) [24] water body index was used to extract the water body features of the images. The formula for SDWI is as follows:

$$\mathrm{SDWI} = \ln(10 \times VV \times VH) - 8 \quad (1)$$

Where VV represents the VV polarization channel of SAR image, VH represents the VH polarization channel of SAR image.

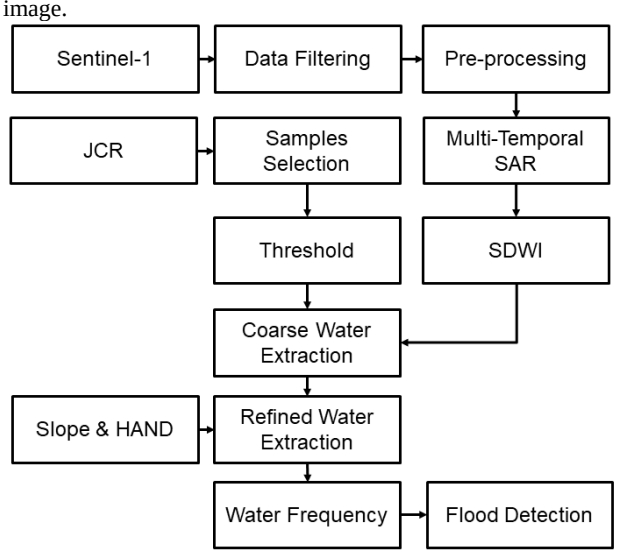


**Figure 2 Flowchart of this study.**

The water body extraction accuracy of sentinel-1 images is constrained by the imaging of SAR images and other factors, and the threshold of water and land separation is also not fixed. Thus we used randomly selected permanent water body samples from the Joint Research Centre (JRC) Global Surface Water datasets to statistically analyse the SDWI in the SAR images. Filter all permanent water samples for SDWI outliers, i.e., values greater than 1 and less than 0. Assuming that the SDWI value coverage of the water body conforms to a normal distribution, the optimal threshold is obtained by calculating the mean SDWI value of all samples and subtracting twice the standard deviation. Through the statistical analysis, the optimal threshold of water was used for rough extraction of water bodies from SAR images.

The accuracy of water bodies extracted using only the threshold segmentation method is not high because there are a large number of mountain shadows in the SAR images in areas with large terrain relief. There is a serious misclassification problem between shadows and water bodies of SAR images in water body extraction, thus we introduced Slope data in Digital Elevation Model (DEM) data and Height Above the Nearest Drainage (HAND) data as the basis for distinguishing water bodies and shadows. After masking the area with slope greater than 20 and HAND greater than 20, we get relatively fine water extraction results.

After extracting the water bodies from the SAR images of each time phase from January 2022 to July 2022, we can obtain the multi-temporal water body results of the Beijiang River basin in the Pearl River. The water frequency statistics are calculated at the pixel level for the water body extraction results of multiple temporal. The water frequency equation is shown below:

$$\mathrm{F} = (N_w)/(N_{All}) * 100\% \quad (2)$$

Where F represents the frequency value of the water body, $N_w$ represents the sum of images of a pixel identified as water in all time phases, and $N_{All}$ represents the sum of images of that pixel. With seasonal changes, the area where the surface is a water body changes considerably during the year. The boundary areas of water bodies change during periods of high and low water. Areas where the surface is covered by water for a long period of time can be classified as permanent water bodies. Therefore, the identification of permanent water bodies is performed based on the water body frequency map F.

The F threshold for determining whether it is a permanent water body varies with the specific geographical location of different regions. By comparing with the JRC data analysis, it was revealed that the area can be identified as permanent water bodies when the frequency of the water body is greater than 60%.Thus, this region uses 60% as the reference threshold. When F is less than a certain reference value and the area of the water body is significantly enlarged, flooding is more likely to occur in the region. By identifying the category of water bodies from SAR images at the time of possible flooding, a large-scale flood detection mapping can be quickly obtained

## 3. RESULTS

During watershed flood disasters, there is a correlation between upstream and downstream floods. Therefore, it is necessary to use remote sensing images to realize global flood dynamic monitoring. In order to verify the effectiveness of the proposed method, the experimental section takes the large-scale flood disaster in the Pearl River in China in June 2022 as an example to monitor the flood disaster range in the Beijiang River Basin. We took Beijiang in the Pearl River Basin as the area of interest and retrieved a total of 70 Sentinel 1 SAR images from January to July 2022. Using the GEE platform to quickly realize the mosaic of time series remote sensing images in the study area. After that, we performed terrain correction pre-processing on the SAR image set using NASA Shuttle Radar Topography Mission (SRTM) digital elevation data, and image noise filtering using RefinedLee algorithm. The above pre-processing operations can remove the interference of some noise and hill shadows on water extraction. 100 points of water body types in the JRC were randomly selected, and the backscattering coefficients of the SAR image set were statistically analyzed according to the point information. Finally, the segmentation threshold of the optimal backscattering coefficient for water extraction in this area can be obtained. The water bodies of long-time series SAR images are extracted by threshold

segmentation method, and hill shadows are removed by topographic data. After the water frequency map is calculated from the multi-temporal water extraction results, the flood disaster area in the Pearl River Basin can be extracted. The results of water body type identification and flood intrusion extent of the whole Beijiang basin can be obtained within a few minutes. June 20 was the most severely affected day in the study area, but since there was no SAR image coverage on that day, flood extent mapping was performed on the June 14 image, when the flooding had just begun. The detection results of the flood disaster range in the Beijiang River Basin are shown in the Figure 3.

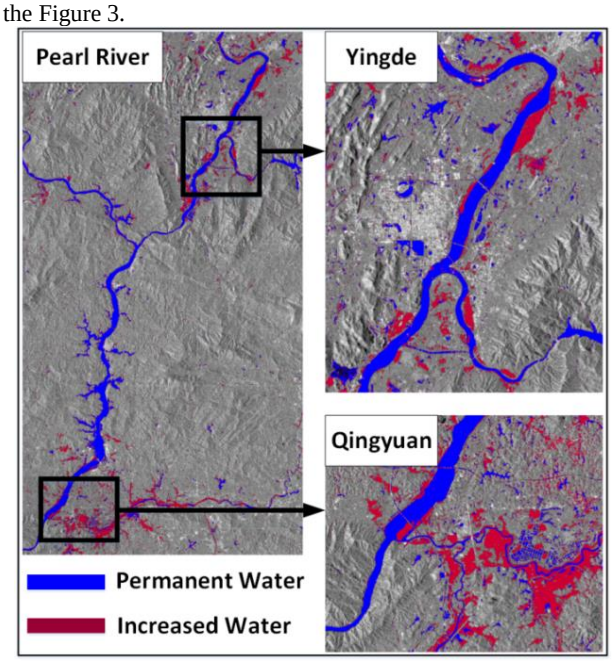


**Figure 3 The extent of flooding in the Beijiang basin of the Pearl River.**

Blue areas are identified permanent water bodies, where the frequency of water bodies is greater than 60%. The red areas are the extent of the increased water body on June 14. The map on the left shows the distribution of flooding in the Beijiang River basin of the entire Pearl River. The right two images are flood detection maps around Yingde City and around Qingyuan City, which were severely attacked by floods in the Pearl River Basin. As can be seen from the Figure 3, there are a large number of increased water bodies around Yingde city and Qingyuan city. The extent of the increased water bodies in Qingyuan is greater than the extent of the increased water bodies in Yingde, and all distributed in the tributary basins of the Beijiang River. The flooded areas are located at the confluence of rivers that are most obvious in Qingyuan City. In the middle reaches of the Beijiang River, both sides of the river are mountainous areas, with no obvious new water body areas.

By mapping the flooding of the entire Beijiang River, it is an important to judge the development of the whole flood disaster., It also can be seen that the proposed method effectively removes the shadow interference in the study area, and the boundaries of permanent and flooded water bodies are clear.

In order to show the development of floods more clearly, the extent of water bodies during the period before and after the floods in Yingde and Qingyuan were mapped. The results are shown in Figure 4 and Figure 5.

The blue area in the figure is the result of water body extraction at different moments. It is obvious that the water expanded significantly on June 14, and the area of the water body on the 26th was significantly less than the area of the water body on the 14th. This is consistent with the fact that June 20 was the most serious flooding event in many parts of the Beijiang River basin. The terrain around the study area of Yingde City is complex, and the range of water bodies extracted by the proposed method effectively suppresses the interference of mountain shadows.

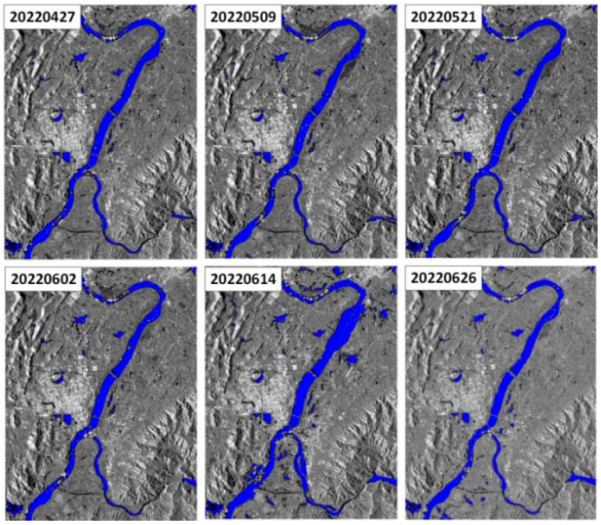


**Figure 4 Water body extraction results of Yingde.**

From the multi-temporal water body extraction results, we can see that the edge information of lakes and other types of blocky water bodies is well maintained. The river area in Figure 4 is effectively extracted as a water body area, and by comparing the water body extraction results of different period, it can be concluded that the permanent water body in Figure 3 is correctly discriminated. The scope of water bodies in Yingde City on June 26 basically restored to the same distribution of water bodies before the flood. Upstream new water bodies recede more quickly compared to downstream receding. There were still large bodies of water in Qingyuan City on June 26, which is in the downstream. Combining the multi-temporal water body extraction results and the flood distribution range during the flood, it is clear to see the flood development status of the affected area.

In addition, it can be seen that the proposed method effectively solves the problem of false detection of water bodies in Qingyuan City due to terrain ups and downs. However, the June 2 image of Qingyuan City has some errors in the water extraction results due to imaging quality problems. The time-series water distribution maps obtained based on the GEE platform provide more information on the development of flooding. As shown in Figure 3, the permanent water bodies in the region are correctly identified by the processing of the water body frequency map.

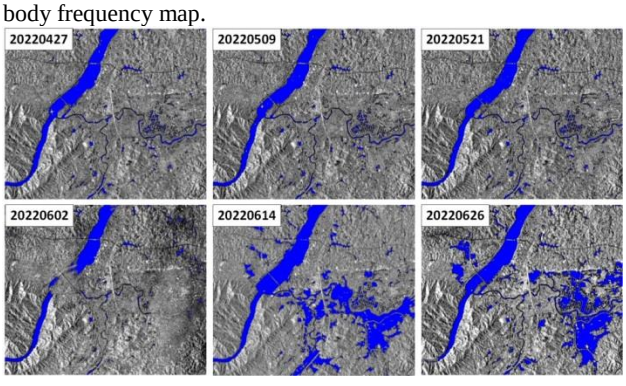


**Figure 5 Water body extraction results of Qingyuan.**

It is difficult to obtain the development status of the disaster from single time phase images due to the development of flood monitoring is very fast. The excellent remote sensing image calculation capability of GEE platform can analyse the time-dimensional information of flood monitoring. The results of water body extraction based on long time series allow obtaining the frequency of water bodies identified as water bodies over a period of time in the study area. The frequency maps of water bodies in Yingde and Qingyuan from January to July 2022 are shown in Figure 6 and Figure 7.

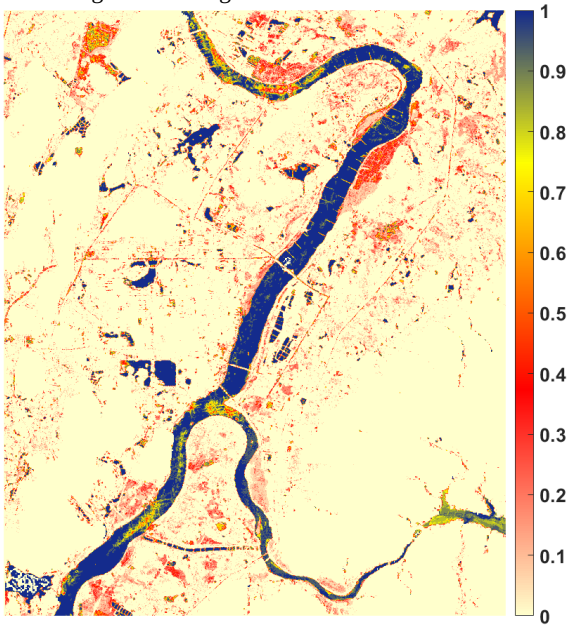


**Figure 6 Frequency map of water bodies of Yingde.**

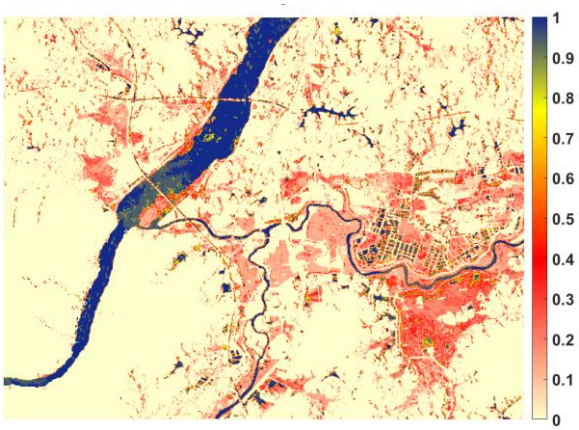


**Figure 7 Frequency map of water bodies of Qingyuan.**

The image represents how often each pixel point was identified as a water body during this period. The closer a pixel value is to 1, the more the pixel can be identified as the permanent water body. The results of water body extractions were considered as seasonal water bodies, except for permanent water bodies. These areas were identified as water bodies less than 60% of the time in the long time series. In the frequency map of water bodies in Yingde, the frequency of water bodies in the river areas are close to 1, while the frequency of water bodies in the area where flooding occurred on June 14 is between 0.1 and 0.5. In addition, the frequency values of water bodies in the road area are approximately between 0.1 and 0.2, indicating that roads are also mixed into water bodies in the multi-temporal water body extraction results.

However, it can be found that the water body frequency map also has some misdetection problems caused by the shadow of the mountain. Permanent water bodies can be effectively identified using water body frequency values, but the accuracy of water body extraction in a single time phase affects the accuracy of flood range detection. Therefore, the selection of thresholds for judging flooding and seasonal water bodies still needs to be further explored.

## 4. CONCULSION

This paper presents a method for large-scale flood monitoring using Sentinel-1 imagery based on the GEE platform. The method makes full use of the multi-temporal information of the Sentinel-1 data to effectively detect the extent of basin flooding and to achieve the distinction between permanent water bodies and new water bodies in flooding.

## ACKNOWLEDGEMENTS

We gratefully acknowledge the European Space Agency (ESA) Copernicus program and the Google Earth Engine for providing SAR and other data and processing capabilities free of charge.

## REFERENCES

Badrinarayanan, V., A. Kendall, and R. Cipolla, *SegNet: A Deep Convolutional Encoder-Decoder Architecture for Image Segmentation.* IEEE Transactions on Pattern Analysis and Machine Intelligence, 2017. **39**(12): p. 2481-2495.

C, G.S., et al., *Dynamic monitoring on flooding situation in the Middle and Lower Reaches of the Yangtze River Region using Sentinel-1A time series.* National Remote Sensing Bulletin, 2021. **25**(10): p. 2127-2141.

Canty, M.J., et al., *Statistical Analysis of Changes in Sentinel-1 Time Series on the Google Earth Engine.* REMOTE SENSING, 2020. **12**(1).

Celik, T., *Unsupervised Change Detection in Satellite Images Using Principal Component Analysis and Means Clustering.* IEEE Geoscience and Remote Sensing Letters, 2009. **6**(4): p. 772-776.

Chen, L.-C., et al. *Encoder-Decoder with Atrous Separable Convolution for Semantic Image Segmentation*. in *Computer Vision – ECCV 2018*. 2018. Cham: Springer International Publishing.

Chini, M., et al., *A Hierarchical Split-Based Approach for Parametric Thresholding of SAR Images: Flood Inundation as a Test Case.* IEEE Transactions on Geoscience and Remote Sensing, 2017. **55**(12): p. 6975-6988.

Chohan, K., et al., *Remote sensing based innovative solution of river morphology for better flood management.* International Journal of Applied Earth Observation and Geoinformation, 2022. **111**: p. 102845.

Dang, B. and Y. Li, *MSResNet: Multiscale residual network via self-supervised learning for water-body detection in remote sensing imagery.* Remote Sensing, 2021. **13**(16): p. 3122.

DeVries, B., et al., *Rapid and robust monitoring of flood events using Sentinel-1 and Landsat data on the Google Earth Engine.* Remote Sensing of Environment, 2020. **240**: p. 111664.

Dong, Z., et al., *Monitoring the summer flooding in the Poyang Lake area of China in 2020 based on Sentinel-1 data and multiple convolutional neural networks.* International Journal of Applied Earth Observation and Geoinformation, 2021. **102**: p. 102400.

Feng, G., et al., *Change detection from synthetic aperture radar images based on neighborhood-based ratio and extreme learning machine.* Journal of Applied Remote Sensing, 2016. **10**(4): p. 1-14.

Gao, Y., et al., *Change Detection From Synthetic Aperture Radar Images Based on Channel Weighting-Based Deep Cascade Network.* IEEE Journal of Selected Topics in Applied Earth Observations and Remote Sensing, 2019. **12**(11): p. 4517-4529.

He, K., et al. *Deep Residual Learning for Image Recognition*. in *2016 IEEE Conference on Computer Vision and Pattern Recognition (CVPR)*. 2016.

Huang, G., et al. *Densely Connected Convolutional Networks*. in *2017 IEEE Conference on Computer Vision and Pattern Recognition (CVPR)*. 2017.

Li, H.-C., et al., *Gabor Feature Based Unsupervised Change Detection of Multitemporal SAR Images Based on Two-Level Clustering.* IEEE Geoscience and Remote Sensing Letters, 2015. **12**: p. 1-5.

Li, L.W., et al., *Water Body Extraction from Very High Spatial Resolution Remote Sensing Data Based on Fully Convolutional Networks.* REMOTE SENSING, 2019. **11**(10).

Li, M., et al., *A Deep Learning Method of Water Body Extraction From High Resolution Remote Sensing Images With Multisensors.* IEEE Journal of Selected Topics in Applied Earth Observations and Remote Sensing, 2021. **14**: p. 3120-3132.

Liang, J. and D. Liu, *A local thresholding approach to flood water delineation using Sentinel-1 SAR imagery.* ISPRS Journal of Photogrammetry and Remote Sensing, 2020. **159**: p. 53-62.

Liu, H., et al., *Annual dynamics of global land cover and its long-term changes from 1982 to 2015.* EARTH SYSTEM SCIENCE DATA, 2020. **12**(2): p. 1217-1243.

Liu, T., et al., *Building Change Detection for VHR Remote Sensing Images via Local–Global Pyramid Network and Cross-Task Transfer Learning Strategy.* IEEE Transactions on Geoscience and Remote Sensing, 2022. **60**: p. 1-17.

Nagai, H., T. Abe, and M. Ohki, *SAR-Based Flood Monitoring for Flatland with Frequently Fluctuating Water Surfaces: Proposal for the Normalized Backscatter Amplitude Difference Index (NoBADI).* Remote Sensing, 2021. **13**(20).

Otsu, N., *A threshold selection method from gray level histograms.* IEEE Transactions on Systems, Man and Cybernetics, 1979. **9**: p. 62-66.

Peter, B.G., et al., *Google Earth Engine Implementation of the Floodwater Depth Estimation Tool (FwDET-GEE) for Rapid and Large Scale Flood Analysis.* IEEE GEOSCIENCE AND REMOTE SENSING LETTERS, 2022. **19**.

Shichao, J., et al., *Study on new method for water area information extraction based on Sentinel-1 data.* Yangtze River, 2019. **50**(02): p. 213-217.

Tulbure, M.G., et al., *Can we detect more ephemeral floods with higher density harmonized Landsat Sentinel 2 data compared to Landsat 8 alone?* ISPRS Journal of Photogrammetry and Remote Sensing, 2022. **185**: p. 232-246.

Vanama, V.S.K. and Y.S. Rao, *Change Detection Based Flood Mapping of 2015 Flood Event of Chennai City Using Sentinel-1 SAR Images*, in *IGARSS 2019 - 2019 IEEE International Geoscience and Remote Sensing Symposium*. 2019. p. 9729-9732.

Wang, J., et al., *Deep High-Resolution Representation Learning for Visual Recognition.* IEEE Transactions on Pattern Analysis and Machine Intelligence, 2021. **43**(10): p. 3349-3364.

Wang, J., et al., *FWENet: a deep convolutional neural network for flood water body extraction based on SAR images.* International Journal of Digital Earth, 2022. **15**(1): p. 345-361.

Wang, Z.B., et al., *MSLWENet: A Novel Deep Learning Network for Lake Water Body Extraction of Google Remote Sensing Images.* REMOTE SENSING, 2020. **12**(24).

Wu, J., et al., *A multiscale graph convolutional network for change detection in homogeneous and heterogeneous remote sensing images.* International Journal of Applied Earth Observation and Geoinformation, 2021. **105**: p. 102615.

Xiaqing, Y., J. Shuanggen, and H. Minmin, *Dynamic changes of main stream water area in the Yangtze River from Sentinel-1 remote sensing data.* Bulletin of Surveying and Mapping, 2022(01): p. 33-38.

Yao, J., et al., *Applications of Stacking/Blending ensemble learning approaches for evaluating flash flood susceptibility.* International Journal of Applied Earth Observation and Geoinformation, 2022. **112**: p. 102932.

Zhang, R., et al., *Mapping homogeneous regions for flash floods using machine learning: A case study in Jiangxi province, China.* International Journal of Applied Earth Observation and Geoinformation, 2022. **108**: p. 102717.